arXiv:2503.01450v2 [cs.LG] 4 Mar 2025

POPGym Arcade: Parallel Pixelated POMDPs

Zekang Wang[1,*], **Zhe He**[1,*], **Edan Toledo**[2], **Steven Morad**[1]
{mc45154,mc45189,smorad}@um.edu.mo, ucabtol@ucl.ac.uk

[1]**Faculty of Science and Technology, University of Macau**
[2]**Department of Computer Science, University College London**

[*]**Equal contribution**

Abstract

We introduce POPGym Arcade, a benchmark consisting of 7 pixel-based environments each with three difficulties, utilizing a single observation and action space. Each environment offers both fully observable and partially observable variants, enabling counterfactual studies on partial observability. POPGym Arcade utilizes JIT compilation on hardware accelerators to achieve substantial speedups over CPU-bound environments. Moreover, this enables Podracer-style architectures to further increase hardware utilization and training speed. We evaluate memory models on our environments using a Podracer variant of Q learning, and examine the results. Finally, we generate memory saliency maps, uncovering how memories propagate through policies. Our library is available at https://github.com/bolt-research/popgym_arcade.

1 Introduction

Reinforcement learning (RL) demonstrates remarkable success in solving complex decision-making problems, particularly in fully observable environments (Silver et al., 2016). However, real-world decision-making often involves partial observability, where agents must act based on incomplete or noisy information. Despite its practical importance, partial observability remains understudied in RL research, partially due to the lack of scalable and efficient benchmarks.

Much of the progress in RL relies on standardized benchmarks, such as the Arcade Learning Environment (ALE) (Bellemare et al., 2013) and MuJoCo (Todorov et al., 2012). While these benchmarks have driven significant advancements, they are often fully observable, or become nearly fully observable when considering the last few observations (Machado et al., 2018). This limitation makes it difficult to evaluate algorithms or models that we later apply to realistic, partially observable scenarios. Furthermore, the high sample complexity of modern RL results in the environment bottlenecking the training process (Lu et al., 2024), particularly for on-policy algorithms that require high-throughput simulations (Shacklett et al., 2021).

In this work, we introduce POPGym Arcade, a hardware-accelerated benchmark suite inspired by both POPGym (Morad et al., 2023a) and the ALE. POPGym Arcade contains seven Atari-like environments, with each environment offering both fully observable and partially observable twins. By sharing transition

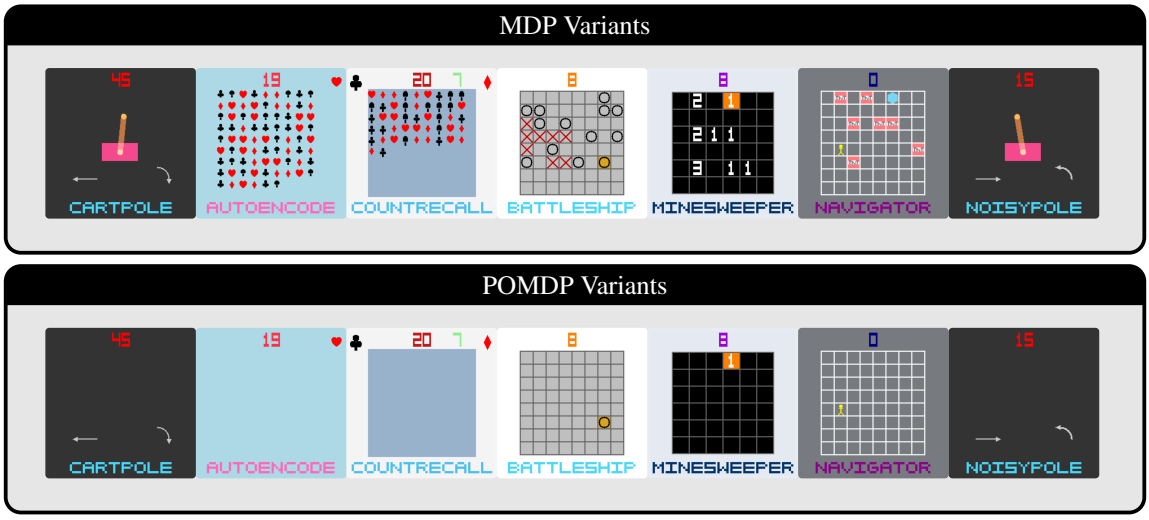


Figure 1: Observations from our environment twins. Observation and actions spaces are shared between all implemented environments, enabling counterfactual studies with observability as the independent variable.

dynamics and observation spaces between all environments and twins, we can isolate and study observability under controlled conditions.

2 Background

In RL, we interact with an environment to maximize the discounted cumulative reward. A Markov Decision Process (MDP) (Sutton & Barto, 2018) is a tuple $\langle S, A, P, R, \gamma \rangle$, with the set of states S, action set A, and state transition function $P : S \times A \mapsto \Delta(S)$, where $\Delta(S)$ corresponds to a distribution over the state space. MDPs also contain a reward function $R : S \times A \mapsto \mathbb{R}$ and discount factor $\gamma \in [0, 1]$. At each timestep, we receive a state s_t and select an action from a policy $a_t \sim \pi(s_t)$ that takes us to the next state following $P(s_{t+1} \mid s_t, a_t)$ while emitting a reward $r_t = R(s_t, a_t)$. We aim to learn the policy $\pi : S \mapsto \Delta(A)$ that maximizes the expected cumulative reward $\mathbb{E}_\pi[\sum_{k=0}^{\infty} \gamma^k R(s_t, a_t) \mid s_0 = s]$.

2.1 Partially Observable Markov Decision Processes

In many realistic scenarios, the agent does not have access to the full state of the environment, instead perceiving portions of the state through noisy or limited sensors. We call this problem setup a Partially Observable Markov Decision Process (POMDP). A POMDP is an extension of the MDP, consisting of tuple $\langle S, A, P, R, \gamma, \Omega, O \rangle$, with the set of observations Ω and the observation function $O : S \mapsto \Delta(\Omega)$. At each timestep, the agent can only access the current observation $o_t \sim O(s_t)$. The observation is not guaranteed to be Markov, thus providing only partial observability of the state, and preventing naive application of standard RL approaches to POMDPs. Fortunately, the sequence of all prior observations and actions, known as the trajectory $\mathbf{x}_t = (o_0, a_0, o_1, a_1 \ldots a_{t-1}, o_t)$, is itself Markov (Sutton & Barto, 2018). As such, an optimal policy must consider all prior observations and actions.

2.2 Memory and Recurrences

For POMDPs, the optimal policy must be a function of a variable length trajectory $\mathbf{x}_t$. For conciseness, we introduce the combined observation-action space $X = (\Omega, A)$ and represent the observation and previous action as $x_t = (o_t, a_{t-1})$.

It is cumbersome to learn a policy over a variable size $\mathbf{x}_t$. We find it simpler to introduce a memory model f that produces a fixed-size latent Markov state $\hat{s} \in \hat{S}$ from the trajectory $\mathbf{x}_t$. This confines the complexities associated with partial observability to f, allowing our policy to operate on a latent Markov state $\hat{s}$. More formally, a recurrent memory model $f : X \times H \mapsto \hat{S} \times H$ maintains a summary of the trajectory in the recurrent state $h \in H$ and outputs a latent Markov state $\hat{s} \in \hat{S}$ for the policy

$$\hat{s}_t, h_t = f(x_t, h_{t-1}) \qquad\qquad a_t \sim \pi(\cdot \mid \hat{s}_t). \tag{1}$$

Associative Recurrences Associative recurrent models, also known as linear recurrent models or memoroids (Morad et al., 2024), utilize a recurrent update $\bullet$ that obeys the associative property

$$s_3, h_3 = (x_1 \bullet x_2) \bullet x_3 = x_1 \bullet (x_2 \bullet x_3). \tag{2}$$

Given a recurrent associative update, we can leverage the associative property to rearrange the order of operations. For example, given four inputs x_1, x_2, x_3, x_4, we can compute either

$$s_4, h_4 = (((x_1 \bullet x_2) \bullet x_3) \bullet x_4) \qquad\qquad s_4, h_4 = (x_1 \bullet x_2) \bullet (x_3 \bullet x_4). \tag{3}$$

The former case corresponds to standard recurrent networks, relying on the prior recurrent state to compute the current state, resulting in linear time complexity. In the latter case, we can compute $x_1 \bullet x_2$ and $x_3 \bullet x_4$ in parallel, achieving logarithmic parallel time complexity (Hinze, 2004). Blelloch (1990) provide an associative scan implementation with linear space complexity.

State-Space Models State-Space Models (SSMs) (Gu et al., 2022) model an associative recurrence via

$$h_t = \overline{A} h_{t-1} + \overline{B} x_t \qquad\qquad \hat{s}_t = \overline{C} h_t + \overline{D} x_t, \tag{4}$$

where $\overline{A}, \overline{B}, \overline{C}, \overline{D}$ are discretizations of carefully initialized trainable parameters A, B, C, D. In practice, we initialize A, B, C, D deterministically. Deterministic initialization applied to many consecutive SSM layers can result in instabilities, and so Orvieto et al. (2023) proposes a meticulously derived random initialization and new parameterization of SSM parameters. They call their method the Linear Recurrent Unit (LRU).

Minimal Recurrent Networks Feng et al. (2024) revisit the popular Gated Recurrent Unit (GRU) (Chung et al., 2014) and Long Short-Term Memory (LSTM) (Hochreiter & Schmidhuber, 1997) RNNs. They simplify the GRU and LSTM recurrent updates, proposing the MinGRU and MinLSTM with efficient associative recurrent updates. The authors write the MinGRU as

$$h_t = (1 - \sigma(Ax_t + b)) \odot h_t + \sigma(Ax_t + b) \odot \tanh(Cx_t + d) \qquad\qquad \hat{s}_t = h_t, \tag{5}$$

with trainable parameters A, b, C, d, sigmoid function σ, and elementwise product $\odot$. The authors find that the MinGRU outperforms multiple SSM variants across offline reinforcement learning tasks, using a decision transformer (Chen et al., 2021) architecture. We note that the decision transformer optimization objective differs from standard policy gradient or value learning objectives. It is not immediately clear how the MinGRU performs on more traditional value estimation or online RL tasks.

2.3 JAX and Hardware Acceleration

JAX (Bradbury et al., 2018) is a numerical computing library, supporting automatic differentiation, just-in-time compilation, vectorization, and parallelization. JAX inspects python functions and translates them to XLA bytecode for hardware-specific Just-In-Time (JIT) compilation. XLA compilation targets include CPUs, Tensor Processing Units (TPUs), GPUs and more. The compiler optimizes and fuses XLA operations to reduce latency and improve throughput. In RL, compiling the environment and algorithm together enables optimizations across the environment-agent interface.

3 Related Work

Progress in RL builds upon a large collection of MDPs and POMDPs (Table 1). Hausknecht & Stone (2015) gauge LSTM on the ALE benchmark, finding that the LSTM underperforms a simpler framestack model that considers the last four observations in almost all environments and suggesting that partial observability is not a big factor in Atari games. Burda et al. (2022) find that even difficult Atari games like Montezuma's Revenge are close to fully observable. These findings line up with Machado et al. (2018), which introduce difficulties to weaken the observability of Atari. Similarly, Ni et al. (2022) mask positions and velocities in the popular MuJoCo (Todorov et al., 2012) benchmark to induce partial observability. Morad et al. (2023b) find that even memory-free policies can perform well on certain masked control tasks.

We call Atari or masked control tasks that admit near-optimal solutions without memory as weak POMDPs. We also include tasks that require minimal effort to induce full observability (e.g., the last four observations is a Markov state). We are interested in strong POMDPs, where long-term memory is necessary for good performance. More recent work propose strong POMDPs specifically to probe the capabilities of reinforcement learning under partial observability. Such work includes navigation tasks (Chevalier-Boisvert et al., 2018; Beattie et al., 2016; Kempka et al., 2016), psychological experiments (Fortunato et al., 2019), as well as party games (Pleines et al., 2022). Unfortunately, training memory models is expensive, making large scale strong POMDP studies rare (Morad, 2024). Morad et al. (2023a) propose POPGym, a set of POMDPs with low dimensional observation spaces. Unfortunately, the simplified observation spaces make it unclear if POPGym-tested methods will transfer to more complex domains, such as pixel-based tasks. Pixel feature extraction and memory are separate tasks, but combining the two could lead to new emergent capabilities (Reed et al.).

Hardware-Accelerated RL Copying data from CPU-based environments to GPU-based policies is a major bottleneck in RL (Lu et al., 2022). Using JAX, one can implement, vectorize (duplicate), and compile their environments directly on accelerator hardware. By executing both the training algorithm and environments on-device, users avoid cpu-to-accelerator copies, training their policies up to one thousand times faster (Lange, 2022; Koyamada et al., 2023; Bonnet et al., 2024; Matthews et al., 2024b). We highlight Matthews et al. (2024a); Pignatelli et al. (2024) which offer hardware-accelerated strong POMDPs. Lu et al. (2024) reimplement POPGym in JAX, achieving even greater efficiency.

One may wonder what effect improved sample throughput has on algorithms research. Hessel et al. (2021) propose the Podracer paradigm for policy search, targeting high sample throughput scenarios. Podracer algorithms include variants of policy gradient (Lu et al., 2022) and PPO (Lange, 2022; Lu et al., 2024; Toledo, 2024). In this work, we focus on the PQN algorithm (Gallici et al., 2024), a simplified parallel version of Q learning. Unlike DQN (Mnih et al., 2015), PQN does not use target networks or replay buffers, and opts for on-policy TD(λ) objective.

Table 1: Related benchmarks and their characteristics. A tilde in the MDP Twins columns means that MDP and POMDP twins do not share observation spaces, making causal studies difficult.

Benchmark	Strong POMDPs	MDP Twins	Pixel Obs.	GPU
MuJoCo/MJX (Todorov et al., 2012)				✓
Atari/ALE (Bellemare et al., 2013)			✓	
DMLab (Beattie et al., 2016)	✓		✓	
VizDoom (Kempka et al., 2016)	✓		✓	
MiniGrid (Chevalier-Boisvert et al., 2018)	✓			
Memory Task Suite (Fortunato et al., 2019)	✓		✓	
MinAtar (Young & Tian, 2019)			✓	
CuLE (Dalton & frosio, 2020)			✓	✓
EnvPool Weng et al. (2022)			✓	✓
Gymnax (Lange, 2022)	✓		✓	✓
POMDP Baselines (Ni et al., 2022)	✓	∼		
MemoryGym (Pleines et al., 2022)	✓	✓	✓	
POPGym (Morad et al., 2023a)	✓	∼		
PGX (Koyamada et al., 2023)				✓
POPJaxRL (Lu et al., 2024)	✓			✓
Jumanji (Bonnet et al., 2024)			✓	✓
Kinetix (Matthews et al., 2024b)			✓	✓
Craftax (Matthews et al., 2024a)	✓		✓	✓
Navix (Pignatelli et al., 2024)	✓		✓	✓
POPGym Arcade (ours)	✓	✓	✓	✓

4 Approach

In this section, we describe our environment properties and implementation details. All proposed environments have observation space $\Omega = [0, 1]^{256\times256\times3}$ (256×256 pixel color images). Similarly, all environments share the action space $A = \{\text{up}, \text{down}, \text{left}, \text{right}, \text{fire}\}$. We bound the undiscounted return for all environments in $[-1, 1]$ to minimize hyperparameter tuning across tasks. Finally, each environment has three distinct difficulty levels to measure long-term progress in RL.

4.1 Partially and Fully Observable Twins

In our framework, MDP and POMDP environment twins share identical underlying state representations $s \in S$ and transition dynamics $P(s_{t+1} \mid s_t, a_t)$, but exhibit distinct observation functions. For an MDP, the observation is guaranteed to be Markov, while this is not the case for a POMDP. The clear boundary between internal state and observation function allows each environment to function as either a MDP or as a POMDP. One can even change observability mid-episode. With our POMDP-MDP twins, we execute studies with observability as the only independent variable, providing stronger evidence and more credibility.

4.2 Vectorized State Transitions and Rendering

We focus on maintaining high environment throughput. First and foremost, we ensure that all environments are both vectorizable and compilable to leverage hardware acceleration. Beyond this, we find a number of small tricks can improve performance. Pre-caching sprites and their positions upon reset provides noticeable performance gains, and replacing calls to `jax.lax.cond` with `jax.lax.switch` provides increased throughput. See Appendix F for more information.

4.3 Memory Introspection Tools

With pixel observations, one can draw conclusions about how pixels impact value predictions (Greydanus et al., 2018). We implement visualization tools to probe which pixels persist in agent memory, and their impact on Q value predictions. More formally, for any timestep we can compute the latent Markov state $\hat{s}$ and recurrent state h from the observation-actions pairs x: $\hat{s}_t, h_t = f(x_t, h_{t-1})$. After training a policy, we initialize h_0 and scan the greedy max Q policy over the environment (P, O, R), as we would during a rollout: $\hat{s}_t, \mathbf{x}_t = \text{scan}(f, Q, P, O, R)$. Finally, we take the magnitude of the partial derivative of Q values, and backpropagate through time

$$\sum_{a_t \in A} \left| \frac{\partial}{\partial \mathbf{o}_t} Q(\hat{s}_t, a_t) \right| \in \Omega^t = \sum_{a_t \in A} \left| \frac{\partial}{\partial \hat{s}_t} Q(\hat{s}_t, a_t) \begin{bmatrix} \frac{\partial \hat{s}_t}{\partial o_0} & \frac{\partial \hat{s}_t}{\partial o_1} & \dots & \frac{\partial \hat{s}_t}{\partial o_t} \end{bmatrix}^\top \right|. \tag{6}$$

This equation measures how much each pixel from $o_{t-k}; k \in \{0 \dots t\}$ propagates through memory and contributes to the value at time t. Using these tools, we can attribute decisions to specific memories and better understand agent behavior.

5 Experiments

We seek to answer the following questions through experiments. See Appendices A to D for additional results and Appendices G and H for architecture and hyperparameter details. All plot shading represents the 95% bootstrapped confidence interval.

How fast is POPGym Arcade? On one hand, we leverage compilation and vectorization, but on the other hand, we have large pixel observation spaces. We compare the throughput of our environments to other well-known environments over ten random seeds in Fig. 2 on an RTX4090 GPU and Intel I7 13700 CPU.

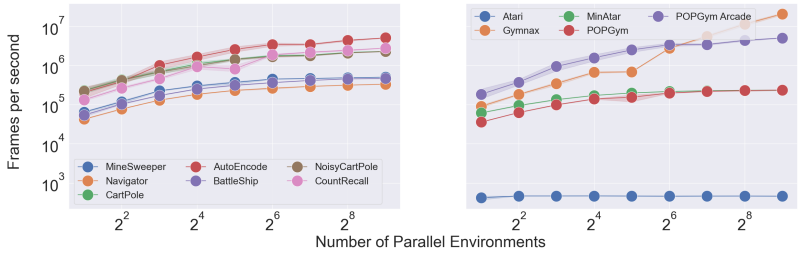
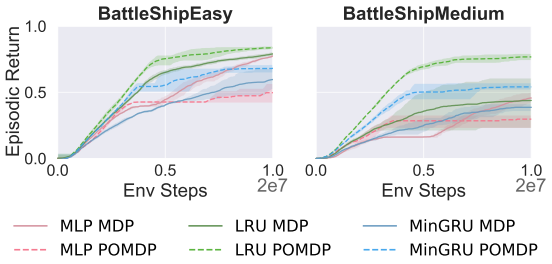


Figure 2: We plot the throughput of our environments in frames per second (FPS), and compare to prior work. We achieve roughly linear scaling with the number of environments, but eventually saturate GPU cores, resulting in sublinear scaling. Still, our method scales better than Atari, and outperforms MinAtar and POPGym benchmarks while producing observations that are orders of magnitude larger.

How does the MinGRU fare in online value estimation? Prior work finds that the MinGRU routinely outperforms SSMs in a decision transformer on offline RL tasks. Does this finding generalize to online RL? In Fig. 3a, we compare the LRU to the MinGRU across all tasks, and provide a breakdown by observability.

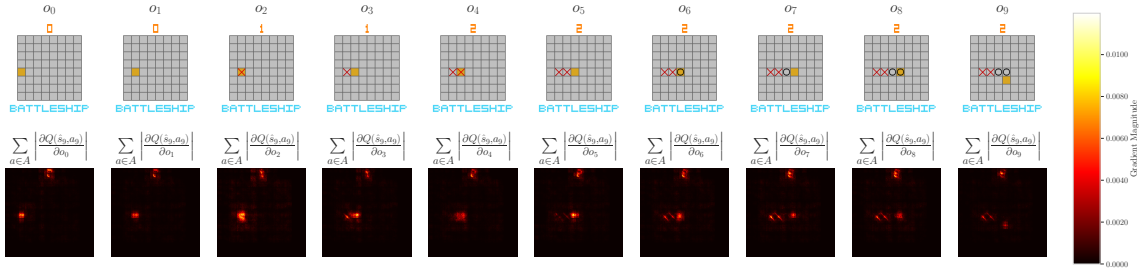
Model	MDP	POMDP	Total
MLP	$\mathbf{0.57} \pm 0.02$	0.33 ± 0.01	0.45 ± 0.01
MinGRU	0.38 ± 0.02	0.45 ± 0.03	0.42 ± 0.02
LRU	0.48 ± 0.06	$\mathbf{0.59} \pm 0.01$	$\mathbf{0.53} \pm 0.04$

(a) The return over all tasks, variants, and difficulties – grouped by model and observability, and reduced using the mean. We represent the standard deviation between seeds. Surprisingly, the MinGRU and LRU tend to perform better on POMDPs than on MDPs.

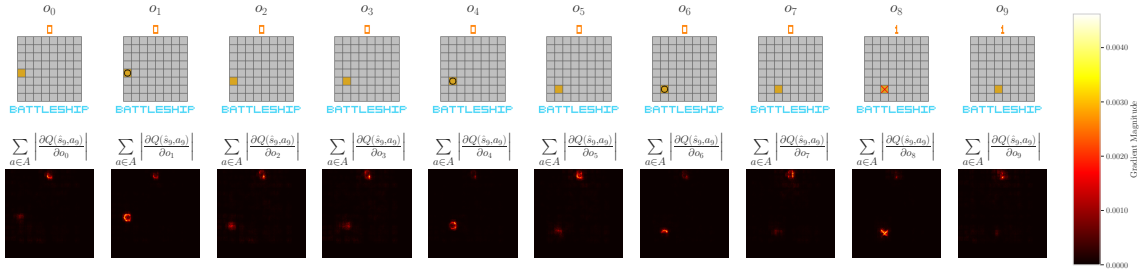


(b) For BattleShip, both MinGRU and LRU provide better sample efficiency under partial observability than full observability.

Figure 3: Comparing POMDP-MDP twins, see Fig. 1 for a visual comparison of environment twins.



(a) **(MDP)** When presented with Markov observations, the policy tends to rely on prior observations to estimate the Q value. The policy bases the Q value on all prior cursor locations, and relies more heavily on the "hit" marker in o_2, o_4 than it does at o_9, the current timestep.



(b) **(POMDP)** The POMDP-trained policy behaves similarly to the MDP, recalling prior hits and misses to estimate the Q value. Here, pixel activations are fewer than the MDP.

Figure 4: Visualization of the LRU, produced by our memory analysis tools. Memory-endowed policies tend to ignore the Markov property.

What role does memory play? Does observability impact behavior? We investigate how our policies utilize memory. With pixel-space observations, we can draw conclusions about how pixels persist in memory, and their impact on Q value predictions. For this experiment, we train for 100M environment steps, until

policies converge (Fig. 13). Then, we use the gradient analysis tools from Section 4.3 to inspect how individual memories impact Q values. We plot the partial derivatives for BattleShip in Fig. 4 (see Appendix B for more tasks).

6 Discussion

POPGym Arcade is fast. Our environments are faster than CPU-based environments and on-par with other GPU-based environments that have much smaller observation spaces. For example, our observations are five orders of magnitude larger than POPGym, yet we run approximately one order of magnitude faster.

SSMs outperform the MinGRU in online value estimation. Although Feng et al. (2024) find that the MinGRU outperforms SSMs in the offline decision transformer setting, our experiments in online value estimation tasks reveal that the LRU SSM delivers superior performance (Fig. 3a). The MLP outperforms both memory models on MDPs, suggesting that memory-endowed policies find suboptimal solutions in the exponentially larger POMDP policy space.

Training memory models on POMDPs can be more efficient than MDPs. In theory, solving POMDPs requires exponentially more training samples than MDPs (Kaelbling et al., 1998), but our empirical evidence suggests otherwise. On average, both the LRU and MinGRU demonstrate slightly better sample efficiency on POMDPs compared to MDPs (Fig. 3a). We drill down into specific tasks in Fig. 3b. We initially suspected POMDP observation aliasing increased policy churn thereby improving exploration (Schaul et al., 2022), but we found this was not the case (Fig. 14). We provide further explanation in the following paragraph.

Memory models ignore the Markov property. Rather than consider POMDPs easy, we should instead consider MDPs difficult. Even in fully observable tasks, recurrent models continue to rely on prior observations to predict Q-values, even when such observations do not affect the return (Fig. 4 and Appendix B). For example, Fig. 5 focuses on past agent positions which do not change the return. This leads us to a fairly surprising finding – given memory, observability is a poor predictor of policy performance. Making a task more or less observable often has less effect on the return than difficulty of the fully observable task (Appendix A). SSMs do not have a prior to emphasize more recent observations. As such, Atari and other weak POMDPs could be sufficiently difficult to evaluate such models.

Limitations We note three limitations of our work. 1. POPGym Arcade rendering logic requires significant GPU memory. We saturate GPU cores with enough parallel environments, resulting in further environments exhibiting sublinear scaling. More powerful GPUs should push this saturation point out further. 2. Fig. 3a uses three random seeds. However, deviation is low between seeds, and most analysis occurs over all environments, providing at least 63 datapoints for each cell in Fig. 3a. 3. We demonstrate that memory models fails to understand the Markov property, but were unable to figure out why this is the case.

7 Conclusion

We proposed the POPGym Arcade benchmark, a collection of parallel pixel-based POMDPs, MDPs, introspection tools, and associative recurrent memory baselines. Using our library, we tested our environments and found that observability might not be as critical to sample efficiency as previously thought.

References

Andrew G. Barto, Richard S. Sutton, and Charles W. Anderson. Neuronlike adaptive elements that can solve difficult learning control problems. *IEEE Transactions on Systems, Man, and Cybernetics*, SMC-13(5): 834–846, 1983. DOI: 10.1109/TSMC.1983.6313077.

Charles Beattie, Joel Z. Leibo, Denis Teplyashin, Tom Ward, Marcus Wainwright, Heinrich Küttler, Andrew Lefrancq, Simon Green, Víctor Valdés, Amir Sadik, Julian Schrittwieser, Keith Anderson, Sarah York, Max Cant, Adam Cain, Adrian Bolton, Stephen Gaffney, Helen King, Demis Hassabis, Shane Legg, and Stig Petersen. DeepMind Lab. Technical Report arXiv:1612.03801, arXiv, December 2016. URL http://arxiv.org/abs/1612.03801. arXiv:1612.03801 [cs] type: article.

M. G. Bellemare, Y. Naddaf, J. Veness, and M. Bowling. The Arcade Learning Environment: An Evaluation Platform for General Agents. *Journal of Artificial Intelligence Research*, 47:253–279, June 2013. ISSN 1076-9757. DOI: 10.1613/jair.3912. URL https://www.jair.org/index.php/jair/article/view/10819.

Guy E Blelloch. Prefix Sums and Their Applications. Technical report, School of Computer Science, Carnegie Mellon University, November 1990.

Clément Bonnet, Daniel Luo, Donal Byrne, Shikha Surana, Sasha Abramowitz, Paul Duckworth, Vincent Coyette, Laurence I. Midgley, Elshadai Tegegn, Tristan Kalloniatis, Omayma Mahjoub, Matthew Macfarlane, Andries P. Smit, Nathan Grinsztajn, Raphael Boige, Cemlyn N. Waters, Mohamed A. Mimouni, Ulrich A. Mbou Sob, Ruan de Kock, Siddarth Singh, Daniel Furelos-Blanco, Victor Le, Arnu Pretorius, and Alexandre Laterre. Jumanji: a Diverse Suite of Scalable Reinforcement Learning Environments in JAX, 2024. URL https://arxiv.org/abs/2306.09884. _eprint: 2306.09884.

James Bradbury, Roy Frostig, Peter Hawkins, Matthew James Johnson, Chris Leary, Dougal Maclaurin, George Necula, Adam Paszke, Jake VanderPlas, Skye Wanderman-Milne, and Qiao Zhang. JAX: composable transformations of Python+NumPy programs, 2018. URL http://github.com/jax-ml/jax.

Greg Brockman, Vicki Cheung, Ludwig Pettersson, Jonas Schneider, John Schulman, Jie Tang, and Wojciech Zaremba. Openai gym, 2016.

Yuri Burda, Harrison Edwards, Amos Storkey, and Oleg Klimov. Exploration by Random Network Distillation. February 2022. URL https://openreview.net/forum?id=H1lJJnR5Ym.

Lili Chen, Kevin Lu, Aravind Rajeswaran, Kimin Lee, Aditya Grover, Misha Laskin, Pieter Abbeel, Aravind Srinivas, and Igor Mordatch. Decision Transformer: Reinforcement Learning Via Sequence Modeling. *Advances in neural information processing systems*, 34:15084–15097, 2021.

Maxime Chevalier-Boisvert, Lucas Willems, and Suman Pal. Minimalistic Gridworld Environment for OpenAI Gym, 2018. URL https://github.com/maximecb/gym-minigrid. Publication Title: GitHub repository.

Junyoung Chung, Caglar Gulcehre, Kyunghyun Cho, and Yoshua Bengio. Empirical evaluation of gated recurrent neural networks on sequence modeling. In *NIPS 2014 Workshop on Deep Learning, December 2014*, 2014.

Steven Dalton and iuri frosio. Accelerating Reinforcement Learning through GPU Atari Emulation. In *Advances in Neural Information Processing Systems*, volume 33, pp. 19773–19782. Curran Associates, Inc., 2020. URL https://proceedings.neurips.cc/paper/2020/hash/e4d78a6b4d93e1d79241f7b282fa3413-Abstract.html.

Leo Feng, Frederick Tung, Mohamed Osama Ahmed, Yoshua Bengio, and Hossein Hajimirsadeghi. Were RNNs All We Needed? October 2024. URL https://openreview.net/forum?id=GrmFFxGnOR.

Meire Fortunato, Melissa Tan, Ryan Faulkner, Steven Hansen, Adrià Puigdomènech Badia, Gavin Buttimore, Charles Deck, Joel Z Leibo, and Charles Blundell. Generalization of Reinforcement Learners with Working and Episodic Memory. In *Advances in Neural Information Processing Systems*, pp. 12448–12457, 2019.

Matteo Gallici, Mattie Fellows, Benjamin Ellis, Bartomeu Pou, Ivan Masmitja, Jakob Nicolaus Foerster, and Mario Martin. Simplifying Deep Temporal Difference Learning, October 2024. URL http://arxiv.org/abs/2407.04811. arXiv:2407.04811 [cs].

Samuel Greydanus, Anurag Koul, Jonathan Dodge, and Alan Fern. Visualizing and Understanding Atari Agents. In *Proceedings of the 35th International Conference on Machine Learning*, pp. 1792–1801. PMLR, July 2018. URL https://proceedings.mlr.press/v80/greydanus18a.html. ISSN: 2640-3498.

Albert Gu, Karan Goel, and Christopher Re. Efficiently Modeling Long Sequences with Structured State Spaces. March 2022. URL https://openreview.net/forum?id=uYLFoz1vlAC.

Matthew Hausknecht and Peter Stone. Deep Recurrent Q-Learning for Partially Observable MDPs. In *2015 AAAI Fall Symposium Series*, September 2015. URL https://www.aaai.org/ocs/index.php/FSS/FSS15/paper/view/11673.

Matteo Hessel, Manuel Kroiss, Aidan Clark, Iurii Kemaev, John Quan, Thomas Keck, Fabio Viola, and Hado van Hasselt. Podracer architectures for scalable Reinforcement Learning, April 2021. URL http://arxiv.org/abs/2104.06272. arXiv:2104.06272 [cs].

Ralf Hinze. An Algebra of Scans. In *Mathematics of Program Construction: 7th International Conference, MPC 2004, Stirling, Scotland, UK, July 12-14, 2004. Proceedings 7*, pp. 186–210. Springer, 2004.

Sepp Hochreiter and Jürgen Schmidhuber. Long Short-Term Memory. *Neural Computation*, 9(8):1735–1780, November 1997. ISSN 0899-7667. DOI: 10.1162/neco.1997.9.8.1735. URL https://doi.org/10.1162/neco.1997.9.8.1735.

Leslie Pack Kaelbling, Michael L. Littman, and Anthony R. Cassandra. Planning and Acting in Partially Observable Stochastic Domains. *Artificial Intelligence*, 101(1-2):99–134, 1998. ISSN 00043702. DOI: 10.1016/s0004-3702(98)00023-x.

Michal Kempka, Marek Wydmuch, Grzegorz Runc, Jakub Toczek, and Wojciech Jaśkowski. ViZDoom: A Doom-based AI Research Platform for Visual Reinforcement Learning. In *IEEE Conference on Computational Intelligence and Games*, pp. 341–348, Santorini, Greece, September 2016. IEEE. URL http://arxiv.org/abs/1605.02097.

Sotetsu Koyamada, Shinri Okano, Soichiro Nishimori, Yu Murata, Keigo Habara, Haruka Kita, and Shin Ishii. Pgx: Hardware-Accelerated Parallel Game Simulators for Reinforcement Learning. In *Advances in Neural Information Processing Systems*, volume 36, pp. 45716–45743, 2023.

Robert Tjarko Lange. gymnax: A JAX-based Reinforcement Learning Environment Library, 2022. URL http://github.com/RobertTLange/gymnax.

Chris Lu, Jakub Kuba, Alistair Letcher, Luke Metz, Christian Schroeder de Witt, and Jakob Foerster. Discovered Policy Optimisation. *Advances in Neural Information Processing Systems*, 35:16455–16468, December 2022. URL https://proceedings.neurips.cc/paper_files/paper/2022/hash/688c7a82e31653e7c256c6c29fd3b438-Abstract-Conference.html.

Chris Lu, Yannick Schroecker, Albert Gu, Emilio Parisotto, Jakob Foerster, Satinder Singh, and Feryal Behbahani. Structured State Space Models for in-Context Reinforcement Learning. *Advances in Neural Information Processing Systems*, 36, 2024.

Marlos C. Machado, Marc G. Bellemare, Erik Talvitie, Joel Veness, Matthew Hausknecht, and Michael Bowling. Revisiting the Arcade Learning Environment: Evaluation Protocols and Open Problems for General Agents. *Journal of Artificial Intelligence Research*, 61:523–562, March 2018. ISSN 1076-9757. DOI: 10.1613/jair.5699. URL https://jair.org/index.php/jair/article/view/11182.

Michael Matthews, Michael Beukman, Benjamin Ellis, Mikayel Samvelyan, Matthew Thomas Jackson, Samuel Coward, and Jakob Nicolaus Foerster. Craftax: A Lightning-Fast Benchmark for Open-Ended Reinforcement Learning. June 2024a. URL https://openreview.net/forum?id=hg4wXlrQCV.

Michael Matthews, Michael Beukman, Chris Lu, and Jakob Foerster. Kinetix: Investigating the Training of General Agents through Open-Ended Physics-Based Control Tasks, October 2024b. URL http://arxiv.org/abs/2410.23208. arXiv:2410.23208 [cs].

Volodymyr Mnih, Koray Kavukcuoglu, David Silver, Andrei A Rusu, Joel Veness, Marc G Bellemare, Alex Graves, Martin Riedmiller, Andreas K Fidjeland, Georg Ostrovski, and others. Human-Level Control Through Deep Reinforcement Learning. *nature*, 518(7540):529–533, 2015. Publisher: Nature Publishing Group.

Steven Morad. *Deep Memory Models and Efficient Reinforcement Learning under Partial Observability*. PhD Thesis, 2024.

Steven Morad, Ryan Kortvelesy, Matteo Bettini, Stephan Liwicki, and Amanda Prorok. POPGym: Benchmarking Partially Observable Reinforcement Learning. In *The Eleventh International Conference on Learning Representations*, 2023a. URL https://openreview.net/forum?id=chDrutUTs0K.

Steven Morad, Ryan Kortvelesy, Stephan Liwicki, and Amanda Prorok. Reinforcement Learning with Fast and Forgetful Memory. *Advances in Neural Information Processing Systems*, 36:72008–72029, December 2023b. URL https://proceedings.neurips.cc/paper_files/paper/2023/hash/e3bf2f0f10774c474de22a12cb060e2c-Abstract-Conference.html.

Steven Morad, Chris Lu, Ryan Kortvelesy, Stephan Liwicki, Jakob Nicolaus Foerster, and Amanda Prorok. Recurrent Reinforcement Learning with Memoroids. November 2024. URL https://openreview.net/forum?id=nA4Q983a1v.

Tianwei Ni, Benjamin Eysenbach, and Ruslan Salakhutdinov. Recurrent Model-Free RL Can Be a Strong Baseline for Many POMDPs. In *Proceedings of the 39th International Conference on Machine Learning*, pp. 16691–16723. PMLR, June 2022. URL https://proceedings.mlr.press/v162/ni22a.html. ISSN: 2640-3498.

Antonio Orvieto, Samuel L Smith, Albert Gu, Anushan Fernando, Caglar Gulcehre, Razvan Pascanu, and Soham De. Resurrecting Recurrent Neural Networks for Long Sequences. In *Proceedings of the 40th International Conference on Machine Learning*, ICML'23. JMLR.org, 2023. Place: Honolulu, Hawaii, USA.

Eduardo Pignatelli, Jarek Liesen, Robert Tjarko Lange, Chris Lu, Pablo Samuel Castro, and Laura Toni. NAVIX: Scaling MiniGrid Environments with JAX, July 2024. URL http://arxiv.org/abs/2407.19396. arXiv:2407.19396 [cs].

Marco Pleines, Matthias Pallasch, Frank Zimmer, and Mike Preuss. Memory Gym: Partially Observable Challenges to Memory-Based Agents. September 2022. URL https://openreview.net/forum?id=jHc8dCx6DDr.

Scott Reed, Konrad Zolna, Emilio Parisotto, Sergio Gómez Colmenarejo, Alexander Novikov, Gabriel Barth-maron, Mai Giménez, Yury Sulsky, Jackie Kay, Jost Tobias Springenberg, and others. A Generalist Agent. *Transactions on Machine Learning Research*.

Tom Schaul, André Barreto, John Quan, and Georg Ostrovski. The phenomenon of policy churn. *Advances in Neural Information Processing Systems*, 35:2537–2549, 2022.

Brennan Shacklett, Erik Wijmans, Aleksei Petrenko, Manolis Savva, Dhruv Batra, Vladlen Koltun, and Kayvon Fatahalian. Large batch simulation for deep reinforcement learning. *CoRR*, abs/2103.07013, 2021. URL https://arxiv.org/abs/2103.07013.

David Silver, Aja Huang, Chris J. Maddison, Arthur Guez, Laurent Sifre, George van den Driessche, Julian Schrittwieser, Ioannis Antonoglou, Veda Panneershelvam, Marc Lanctot, Sander Dieleman, Dominik Grewe, John Nham, Nal Kalchbrenner, Ilya Sutskever, Timothy Lillicrap, Madeleine Leach, Koray Kavukcuoglu, Thore Graepel, and Demis Hassabis. Mastering the game of Go with deep neural networks and tree search. *Nature*, 529(7587):484–489, January 2016. ISSN 1476-4687. DOI: 10.1038/nature16961. URL https://www.nature.com/articles/nature16961. Publisher: Nature Publishing Group.

Richard S Sutton and Andrew G Barto. *Reinforcement Learning: An Introduction*. MIT press, 2018.

Emanuel Todorov, Tom Erez, and Yuval Tassa. MuJoCo: A physics engine for model-based control. In *2012 IEEE/RSJ International Conference on Intelligent Robots and Systems*, pp. 5026–5033, October 2012. DOI: 10.1109/IROS.2012.6386109. URL https://ieeexplore.ieee.org/abstract/document/6386109?casa_token=1tMZ2sK7IroAAAAA:VhBdmpcQ2-7j2n2asoRU2qOZtxjiI3gcLmbFZscPxjgIhe267hBtCSJr_y__QuoXuGvfu0W-. ISSN: 2153-0866.

Edan Toledo. Stoix: Distributed Single-Agent Reinforcement Learning End-to-End in JAX, April 2024. URL https://github.com/EdanToledo/Stoix.

Jiayi Weng, Min Lin, Shengyi Huang, Bo Liu, Denys Makoviichuk, Viktor Makoviychuk, Zichen Liu, Yufan Song, Ting Luo, Yukun Jiang, Zhongwen Xu, and Shuicheng Yan. EnvPool: A Highly Parallel Reinforcement Learning Environment Execution Engine. June 2022. URL https://openreview.net/forum?id=BubxnHpuMbG.

Kenny Young and Tian Tian. MinAtar: An Atari-Inspired Testbed for Thorough and Reproducible Reinforcement Learning Experiments, June 2019. URL http://arxiv.org/abs/1903.03176. arXiv:1903.03176 [cs].

Supplementary Materials

The following content was not necessarily subject to peer review.

A Return Breakdown by Model

Table 2: Return for the LRU model, broken down by task and observability. We also list the absolute difference in return between each MDP/POMDP variant.

Environment	MDP Return	POMDP Return	Absolute Difference
AutoEncodeEasy	0.26 ± 0.00	0.26 ± 0.01	0.00
AutoEncodeMedium	$\mathbf{0.25} \pm 0.00$	0.25 ± 0.00	0.00
AutoEncodeHard	$\mathbf{0.24} \pm 0.00$	0.24 ± 0.00	0.00
BattleShipEasy	0.79 ± 0.01	$\mathbf{0.84} \pm 0.01$	0.05
BattleShipMedium	0.44 ± 0.18	$\mathbf{0.77} \pm 0.02$	0.33
BattleShipHard	0.37 ± 0.21	$\mathbf{0.64} \pm 0.01$	0.27
CartPoleEasy	$\mathbf{0.99} \pm 0.00$	0.99 ± 0.00	0.00
CartPoleMedium	$\mathbf{0.97} \pm 0.02$	0.96 ± 0.02	0.01
CartPoleHard	$\mathbf{0.96} \pm 0.01$	0.91 ± 0.02	0.05
CountRecallEasy	$\mathbf{0.52} \pm 0.01$	0.37 ± 0.00	0.15
CountRecallMedium	$\mathbf{0.24} \pm 0.03$	0.24 ± 0.02	0.00
CountRecallHard	0.19 ± 0.01	$\mathbf{0.21} \pm 0.01$	0.02
MineSweeperEasy	$\mathbf{0.78} \pm 0.00$	0.65 ± 0.04	0.13
MineSweeperMedium	$\mathbf{0.35} \pm 0.02$	0.33 ± 0.02	0.02
MineSweeperHard	0.18 ± 0.01	$\mathbf{0.23} \pm 0.00$	0.05
NavigatorEasy	0.10 ± 0.69	$\mathbf{0.59} \pm 0.01$	0.49
NavigatorMedium	-0.36 ± 0.04	$\mathbf{0.49} \pm 0.02$	0.85
NavigatorHard	-0.17 ± 0.07	$\mathbf{0.48} \pm 0.01$	0.65
NoisyCartPoleEasy	$\mathbf{0.99} \pm 0.00$	0.99 ± 0.00	0.00
NoisyCartPoleMedium	$\mathbf{0.98} \pm 0.00$	0.98 ± 0.00	0.00
NoisyCartPoleHard	0.96 ± 0.00	$\mathbf{0.97} \pm 0.00$	0.01

Table 3: Return for the MinGRU model, broken down by task and observability. We also list the absolute difference in return between each MDP/POMDP variant.

Environment	MDP Return	POMDP Return	Absolute Difference
AutoEncodeEasy	0.27 ± 0.00	$\mathbf{0.28} \pm 0.00$	0.01
AutoEncodeMedium	$\mathbf{0.26} \pm 0.00$	0.26 ± 0.00	0.00
AutoEncodeHard	$\mathbf{0.25} \pm 0.00$	0.24 ± 0.01	0.01
BattleShipEasy	0.60 ± 0.07	$\mathbf{0.68} \pm 0.03$	0.08
BattleShipMedium	0.39 ± 0.02	$\mathbf{0.54} \pm 0.01$	0.15
BattleShipHard	0.31 ± 0.03	$\mathbf{0.43} \pm 0.09$	0.12
CartPoleEasy	$\mathbf{0.96} \pm 0.00$	0.89 ± 0.02	0.07
CartPoleMedium	$\mathbf{0.90} \pm 0.01$	0.72 ± 0.02	0.18
CartPoleHard	$\mathbf{0.87} \pm 0.09$	0.53 ± 0.02	0.26
CountRecallEasy	$\mathbf{0.40} \pm 0.01$	0.23 ± 0.01	0.17
CountRecallMedium	$\mathbf{0.20} \pm 0.01$	0.14 ± 0.04	0.06
CountRecallHard	$\mathbf{0.17} \pm 0.01$	0.09 ± 0.03	0.08
MineSweeperEasy	$\mathbf{0.71} \pm 0.01$	0.55 ± 0.02	0.16
MineSweeperMedium	$\mathbf{0.29} \pm 0.01$	0.24 ± 0.00	0.05
MineSweeperHard	0.14 ± 0.01	$\mathbf{0.15} \pm 0.01$	0.01
NavigatorEasy	-0.49 ± 0.02	$\mathbf{0.48} \pm 0.02$	0.97
NavigatorMedium	-0.47 ± 0.02	$\mathbf{0.36} \pm 0.03$	0.83
NavigatorHard	-0.41 ± 0.02	$\mathbf{0.17} \pm 0.19$	0.58
NoisyCartPoleEasy	$\mathbf{0.96} \pm 0.01$	0.90 ± 0.02	0.06
NoisyCartPoleMedium	$\mathbf{0.92} \pm 0.02$	0.85 ± 0.01	0.07
NoisyCartPoleHard	$\mathbf{0.85} \pm 0.03$	0.76 ± 0.01	0.09

B Additional Memory Analysis

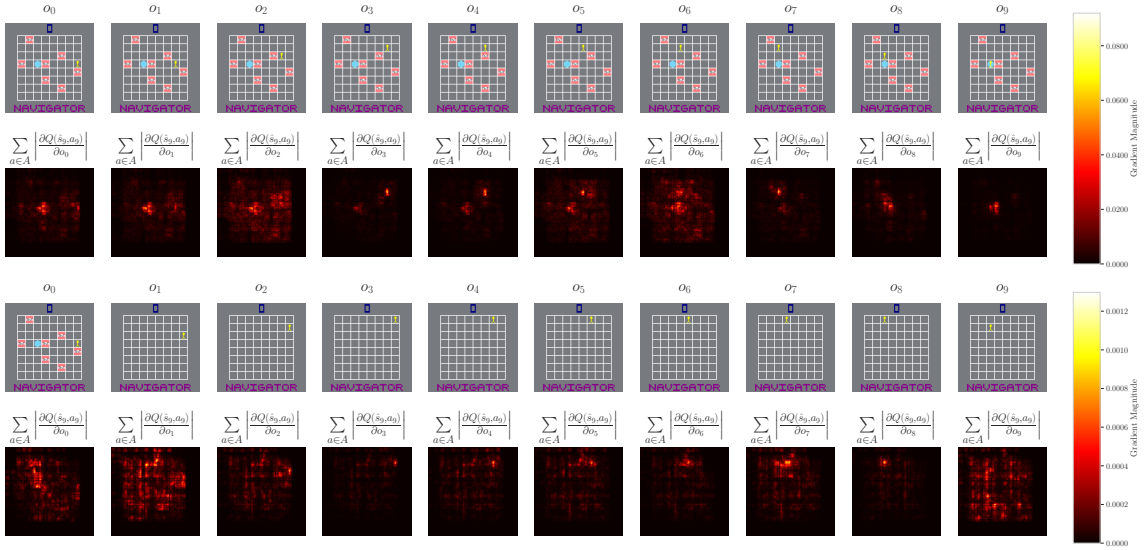


Figure 5: **(MDP, Top)** The MDP-trained policy focuses on the position of the goal and agent position in prior observations, even though this information is unecessary at $t = 9$. In particular, we see the the agent remember explosive tiles from near-death experiences (o_2, o_6), where the shortest path would take the agent through explosive tiles. At the risk of anthropomorphizing, one might consider this the emergence of "fear", or how a traumatic event from the past can persist in memory influence future decision making. **(POMDP, Bottom)** The agent takes a safer path to the goal. At o_9, the agent must head south to reach the goal. In o_0, we see the path from the location at $t = 9$ to the goal highlighted, suggesting the agent is planning an unobstructed path to the goal, using information stored at $t = 0$.

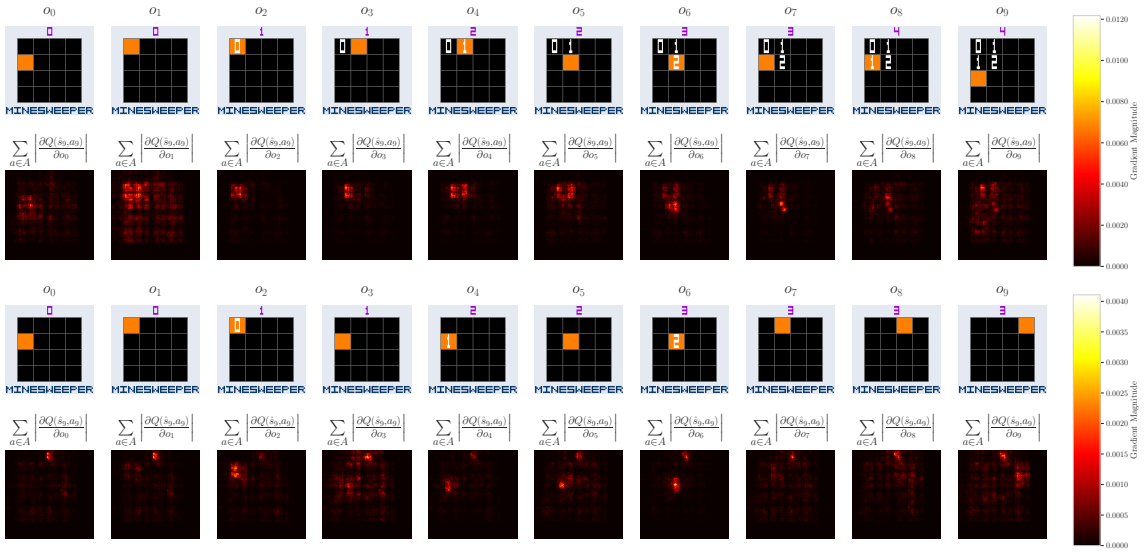


Figure 6: **(MDP, Top)** Like in previous experiments, the MDP policy tends to base Q values on the memory corresponding to prior observations of the tiles. We see larger activations when tiles are first revealed at o_2, o_4, o_6 than the equivalent tiles in o_9. **(POMDP, Bottom)** In the POMDP, the agent memory focuses more heavily on the score at the top of the screen. We see hotspots when tiles are first revealed, demonstrating that the policy remembers the location of previously swept tiles.

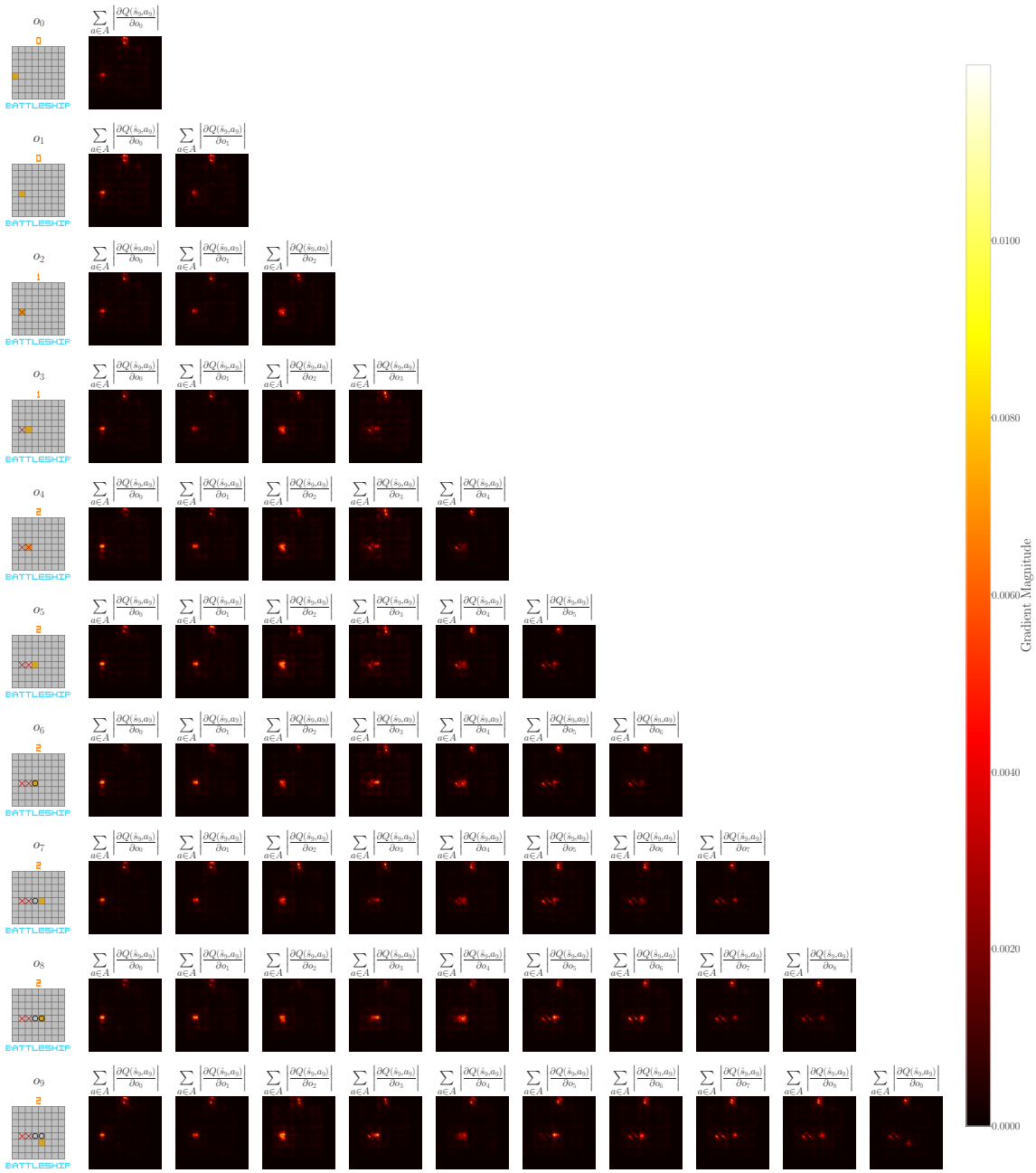


Figure 7: Partial derivative grid for Battleship MDP

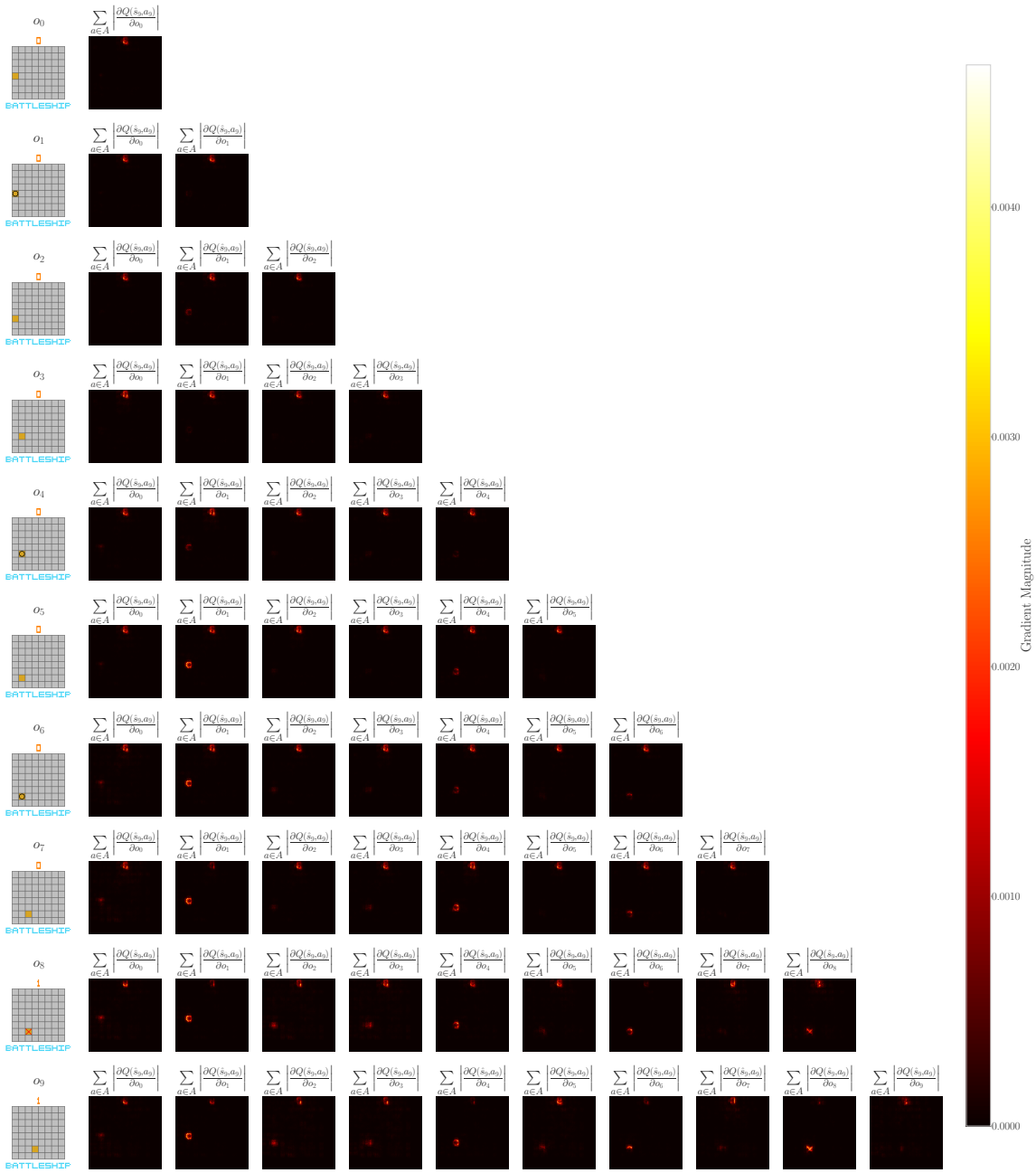


Figure 8: Partial derivative grid for Battleship POMDP

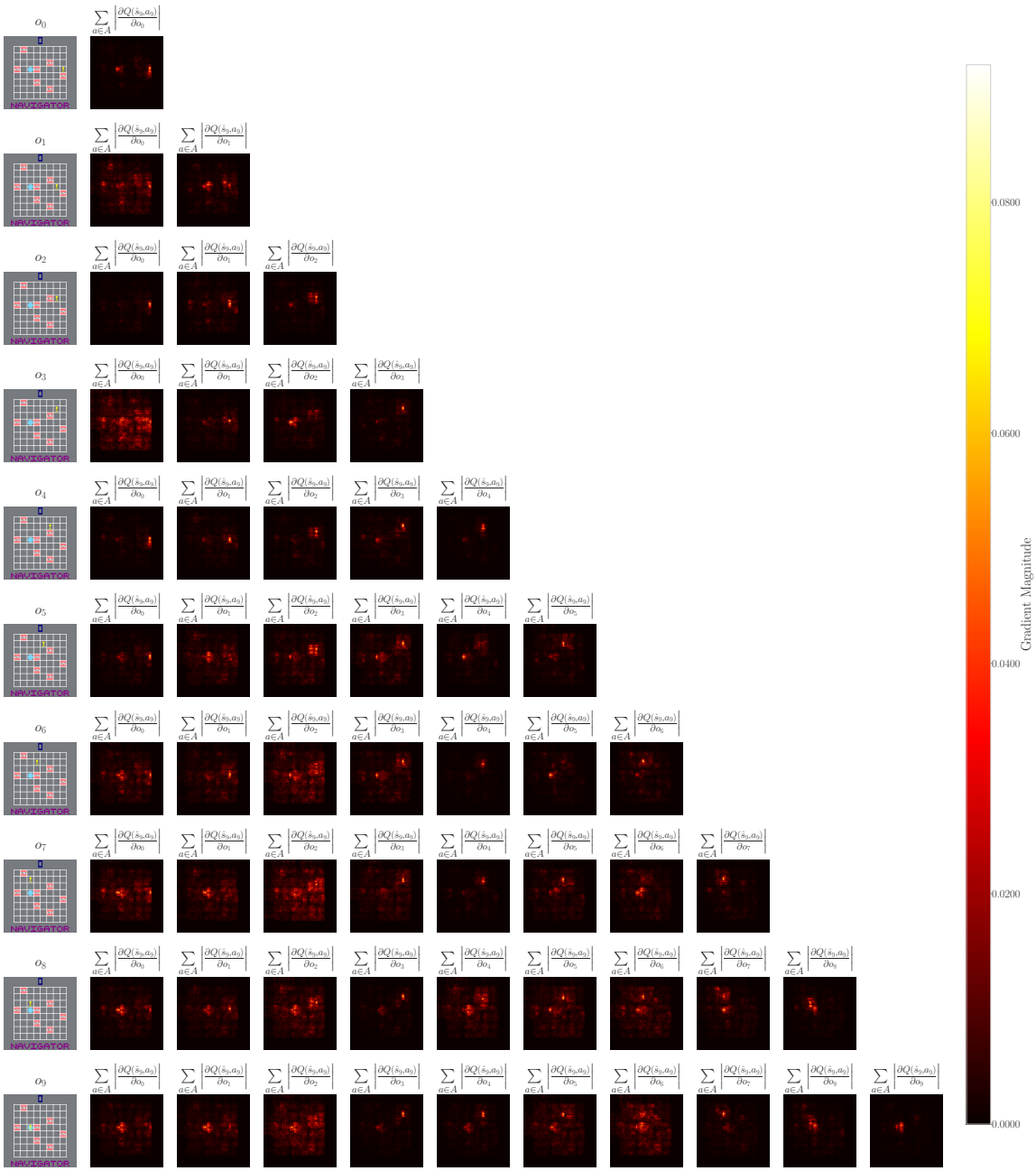


Figure 9: Partial derivative grid for Navigator MDP

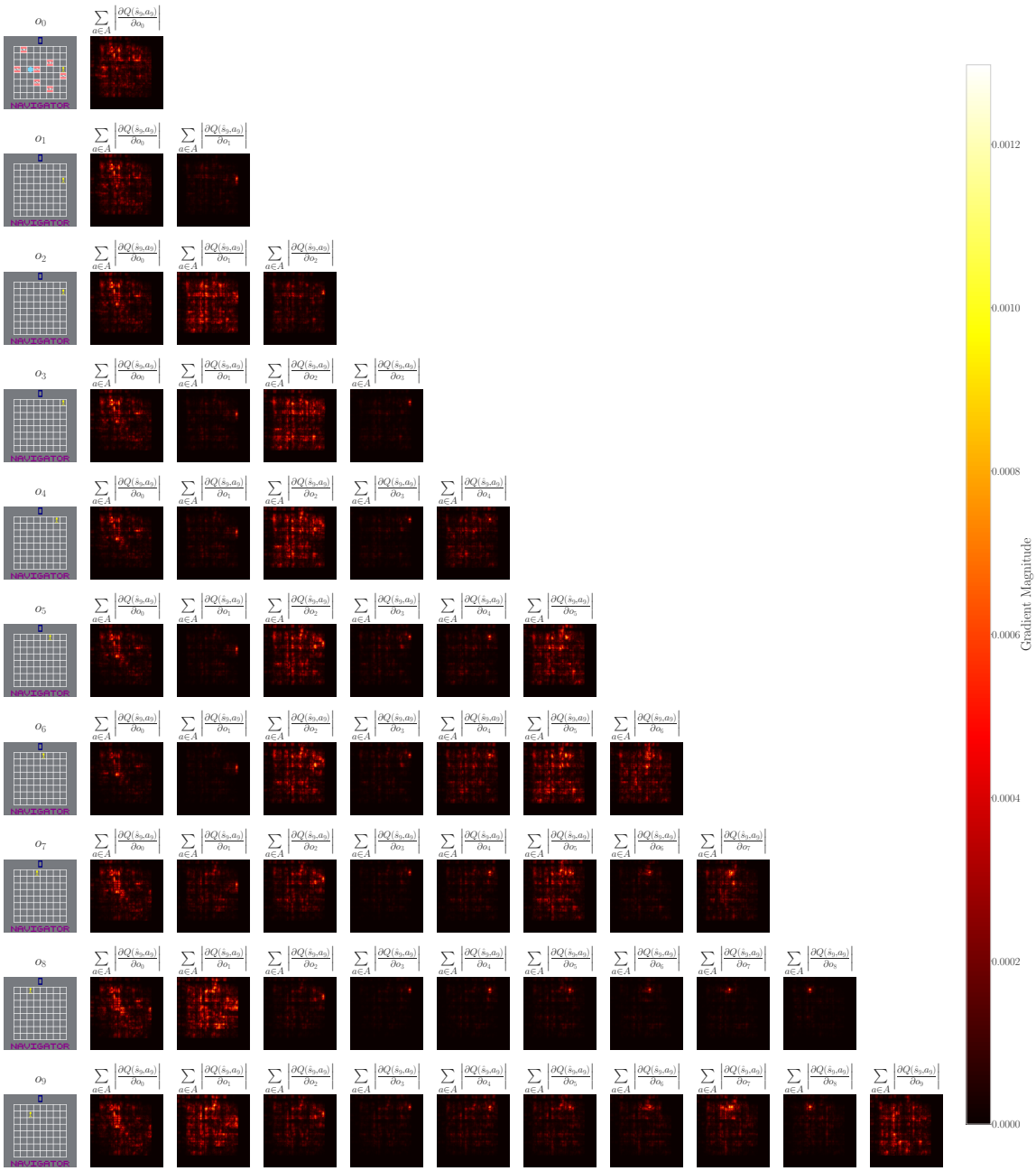


Figure 10: Partial derivative grid for Navigator POMDP

C Return Plots

We present our results as line plots, demonstrating the maximum cumulative episodic reward achieved during each run, separated by environment and the difficulty level (Figs. 11 and 12)

With all the experiments, a sample of 10M timesteps are taken from the respective environment. However, in the case of BattleShip and CountRecall experiments, the sample is set to 20M timesteps.

We use 3 random seed and smooth the line plots using EWMA. The solid area depict the mean and the shaded area is the 95% bootstrap confidence interval.

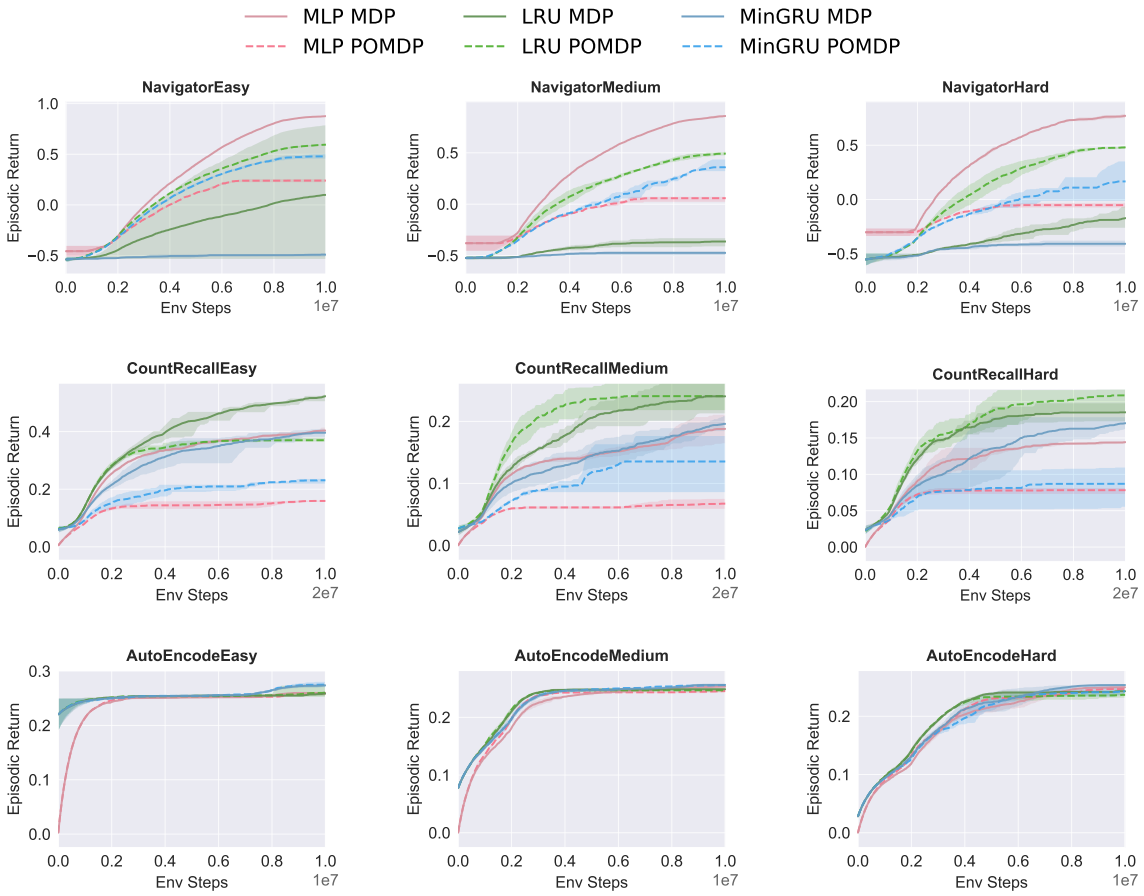


Figure 11: Return plots (continued)

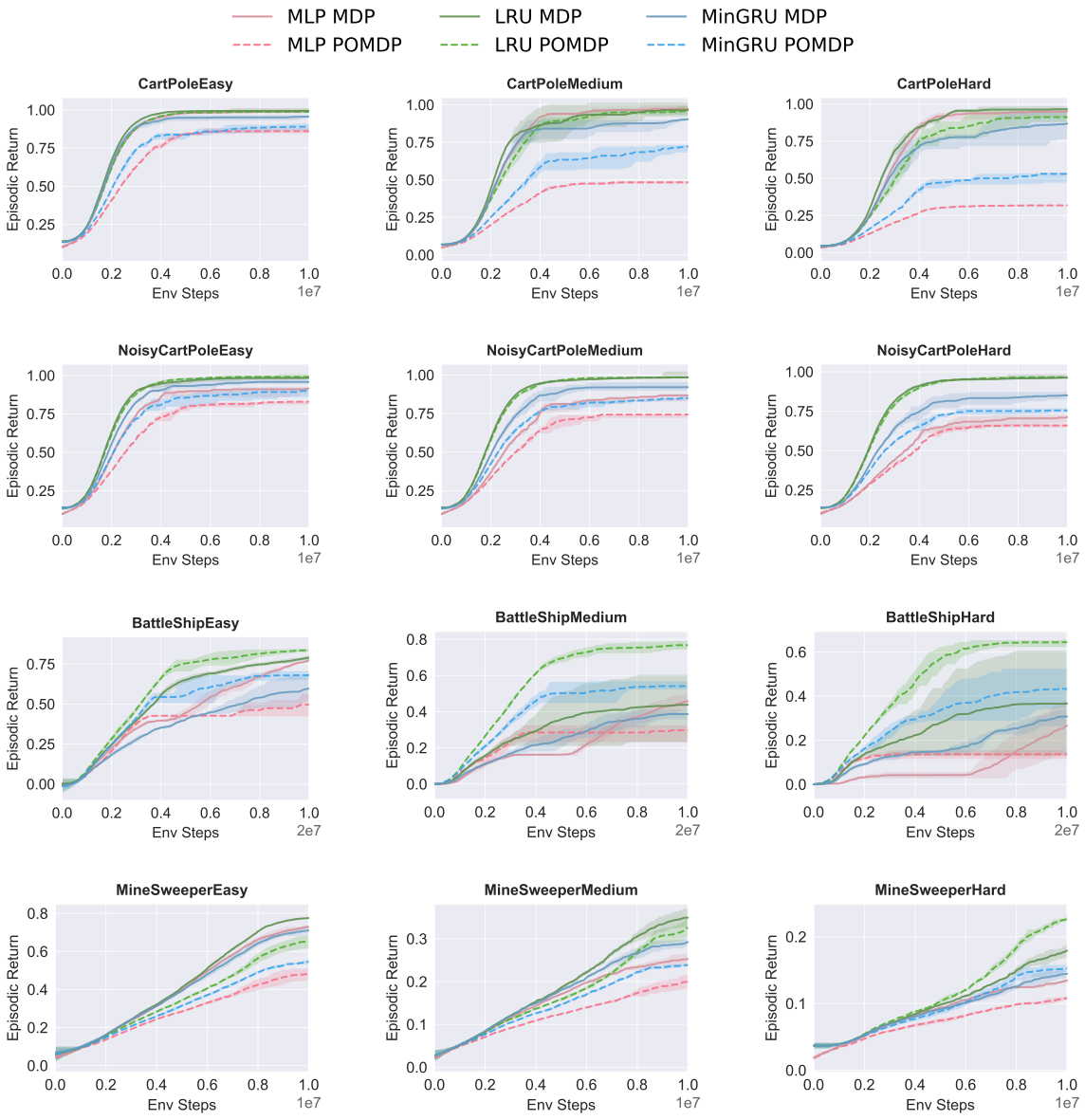


Figure 12: Return plots (continues on next page)

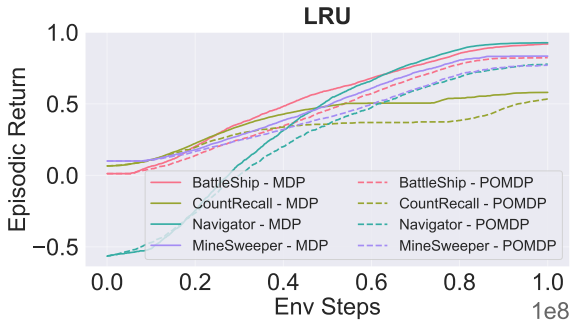


Figure 13: For our gradient analysis, we train the LRU policies for 100M environment steps until convergence.

D Policy Churn

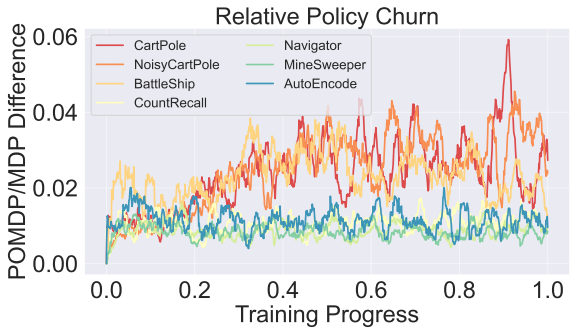


Figure 14: We execute a pilot study to see if policy churn is significantly different between policies trained on POMDPs and MDPs. We plot the difference in churn between the MDP and corresponding POMDP policies. For example, if the POMDP policy has a churn ratio of 0.5 (half of states) and the MDP policy has a churn of 0.4, the difference in churn rates would be 0.1. We see negligible differences in churn between POMDPs and MDPs.

E Environment Descriptions

1. **Stateless Cartpole:** Following the classic cartpole settings from (Barto et al., 1983). Rendered with similar visualization style from (Brockman et al., 2016), but with two indicative figures to represent horizontal speed of cart and angular velocity of pole respectively.
2. **Noisy Stateless Cartpole:** Stateless Cartpole (Env. 1) affected by Gaussian noise on position and speed of the cart as well as angle and angular velocity of the pole.
3. **Battleship:** The agent's goal is to sink all the pre-placed ships to win the game. The agent controls a cursor that represents its current position on the grid. Each turn, the agent can either move the cursor one space or choose to "FIRE" the current grid cell. Each cell can be in one of two states: HIT or MISS. The

agent receives a positive reward for hitting a ship, a neutral reward (0) for the first miss on an empty cell, and a negative reward for repeatedly firing a cell that has already been targeted.

4. **Count Recall:** Every turn, the agent gets a value card and a query card. The agent's task is to figure out how many times the query card has shown up so far. To do this, the agent counts how many times it has received the matching value card and uses that as the answer. If the agent guesses the correct count, it receives a positive reward. If the guess is incorrect, the agent receives no reward (0). This setup encourages the agent to accurately track and recall the frequency of specific cards over time.
5. **Mine Sweeper:** The agent's goal is to hit all the non-mine cells to win the game, inspired by the classic computer game Minesweeper. Similar to Battleship environments, the agent controls a cursor to navigate the grid and can either move to an adjacent cell or "hit" the current cell each turn. Hitting a safe cell earns the agent a positive reward, while hitting a mine results in no reward (0) and ends the game. If the agent tries to hit a cell that has already been revealed, it receives a negative reward. This reward structure encourages the agent to explore efficiently, avoid mines, and minimize redundant actions to maximize its cumulative reward.
6. **Autoencode:** This game is similar to Simon but played in reverse. The agent's task is to recall and replay a sequence of cards in the opposite order they were shown. During the WATCH phase, the agent observes a randomly generated sequence of cards. In the PLAY phase, the agent must reproduce the sequence in reverse order. The agent receives a positive reward for each correct card played and no reward (0) for incorrect choices. This environment tests the agent's ability to encode a series of observations into a latent state and then decode that state step by step to reproduce the sequence accurately.
7. **Navigator:** The agent's goal is to locate and confirm the treasure on the board while avoiding the TNT to win the game. The agent navigates using a cursor that marks its current position. On each turn, it can either shift the cursor to an adjacent cell or decide to confirm the cell it's currently on. Every move the agent makes results in a small negative reward. If the agent lands on a TNT cell, it receives a significant negative reward, and the game ends immediately. This environment challenges the agent to discover the most efficient path to the treasure, aiming to maximize its cumulative reward by completing the game as quickly as possible.

F Vectorized Rendering Details

Our rendering system is built on a canvas framework. We draw to the canvas using primitives, such as letters, numbers, shapes, and more. All rendering functions are pure (without side effects), and may be easily vectorized or compiled. We build our rendering framework on top of `jax.numpy` and does not use any external dependencies. With these tools, anyone can easily render their own custom grid-based or card-based environments for further research and exploration.

Five of seven of our proposed environments come with fairly intricate rules, requiring multiple iterations of pattern rendering on the canvas. These complex tasks can be broadly split into two rendering categories: grid-based environments, like Battleship, and card-based environments, like CountRecall. Initially, we re-rendered at each step, but this was slow, even with JIT compilation. We found that removing dynamic computations improved performance, which we detail below.

Grid-based environment In grid-based games, we divide the entire canvas into a bunch of small square cells, where each cell displays either the same or a unique pattern to reflect the environmental info contained in the current state. We precompute the coordinates of every cell that needs to be drawn on the canvas and

stash them in two matrices – one for the x-axis positions and one for the y-axis. During rendering, we leverage `jax.vmap` to handle the process in parallel along the row dimension.

Card-based environment We precompute all possible card templates (value, query, and historical cards) during initialization period, avoiding repetitive redrawing of static elements like suits or card positions. This turns dynamic rendering into a fast lookup-and-merge process. For example, when rendering value or query cards, we retrieve pre-drawn templates and apply them to the canvas using masks, skipping pixel-by-pixel logic during runtime. For the history display, we vectorize the drawing of historical cards using `jax.vmap`, generating all variations upfront and later selecting only the visible ones with fast array indexing. By JIT-compiling the render function, we lock these optimizations into a highly efficient, hardware-accelerated pipeline. The benefits are reduced per-frame computation, minimal branching, and GPU-friendly operations—all critical for real-time rendering. Even when rendering complex elements like the history grid, we avoid loops and instead use clever indexing with `jnp.argmax` and masks to overlay the latest valid symbols.

G Network Architecture

PQN Our Q-network combines spatial feature extraction with decision policy learning through a JAX/Equinox implementation. The network processes batches of 256×256 RGB images through four convolutional blocks, followed by three dense layers with intermediate normalization (Table 4).

Table 4: Q network architecture

Layer	Parameters	Activation
Conv2D-1	Channels: $3, 64$, Kernel: 7×7, Stride: 2	LeakyReLU
MaxPool2D-1	Pool: 2×2, Stride: 2	–
Conv2D-2	Channels: $64, 128$, Kernel: 3×3, Stride: 2	LeakyReLU
MaxPool2D-2	Pool: 2×2, Stride: 2	–
Conv2D-3	Channels: $128, 256$, Kernel: 3×3, Stride: 2	LeakyReLU
MaxPool2D-3	Pool: 2×2, Stride: 2	–
Conv2D-4	Channels: $256, 512$, Kernel: 3×3, Stride: 2	LeakyReLU
Dense-1	Features: $512, 256$	LeakyReLU
LayerNorm	Shape: 256	–
Dense-2	Features: $256, 256$	LeakyReLU
LayerNorm	Shape: 256	–
Dense-3	Features: $256, 5$	–

PQN $\times$ RNN Our recurrent Q-network extends the base architecture with explicit memory handling through a hybrid CNN-RNN-MLP design. The RNN combines a 512-channel input tensor x with a 5-

dimensional one-hot encoded last action vector from POPGym Arcade, processes these through its 512-unit hidden state, and generates 256-dimensional output features (Table 5).

Table 5: Recurrent Q network architecture

Layer	Parameters	Activation
Conv2D-1	Channels: $3, 64$, Kernel: 7×7, Stride: 2	LeakyReLU
MaxPool2D-1	Pool: 2×2, Stride: 2	–
Conv2D-2	Channels: $64, 128$, Kernel: 3×3, Stride: 2	LeakyReLU
MaxPool2D-2	Pool: 2×2, Stride: 2	–
Conv2D-3	Channels: $128, 256$, Kernel: 3×3, Stride: 2	LeakyReLU
MaxPool2D-3	Pool: 2×2, Stride: 2	–
Conv2D-4	Channels: $256, 512$, Kernel: 3×3, Stride: 2	LeakyReLU
RNN Cell	Input, Hidden, Output: $517, 512, 256$, Num Layer: 1	
Dense-1	Features: $256, 256$	LeakyReLU
LayerNorm	Shape: 256	–
Dense-2	Features: $256, 5$	–

H Experiment Hyperparameters

Table 6: PQN hyperparameters used in all of our experiments. See Gallici et al. (2024) for a detailed description of hyperparameters.

Parameter	**Value**
TOTAL_TIMESTEPS	10e6,20e6,100e6
TOTAL_TIMESTEPS_DECAY	1e6,2e6,20e6
NUM_ENVS	16
MEMORY_WINDOW	4
NUM_STEPS	128
EPS_START	1.0
EPS_FINISH	0.05
EPS_DECAY	0.25
NUM_MINIBATCHES	16
NUM_EPOCHS	4
NORM_INPUT	False
NORM_TYPE	layer norm
LR	0.00005
MAX_GRAD_NORM	0.5
LR_LINEAR_DECAY	True
REW_SCALE	1.0
GAMMA	0.99
LAMBDA	0.95